AJNR Am J Neuroradiol 26:442–446, March 2005

Histopathologic Correlates of Radial Stripes on MR Images in Lysosomal Storage Disorders

J. Patrick van der Voorn, Petra J. W. Pouwels, Wout Kamphorst, James M. Powers, Martin Lammens, Frederik Barkhof, and Marjo S. van der Knaap

BACKGROUND AND PURPOSE: **Radially oriented hypointense stripes in hyperintense cerebral white matter are recognized on T2-weighted images of certain lysosomal storage disorders. We compared *in vivo* and postmortem MR imaging with histopathologic findings in three patients with metachromatic leukodystrophy (MLD), globoid cell leukodystrophy (GLD), and infantile GM1 gangliosidosis (GM1) to understand this characteristic MR imaging pattern.**

***METHODS*: The *in vivo* MR imaging protocol comprised T1- and T2-weighted spin-echo and fluid-attenuated inversion recovery imaging. Postmortem MR imaging, including coronal 1-cm-thick brain sections, was performed after at least 5 weeks of formalin fixation and included T2-weighted spin-echo images and 3D fluid-attenuated inversion recovery images with high spatial resolution. Afterward, the sections were embedded in paraffin, whole-mount sections were made, and neuropathologic stains were applied.**

RESULTS: **Similar imaging features were found in the three patients on *in vivo* and postmortem images, with more prominent stripes in GLD and MLD than in GM1. Neuropathologic examination revealed that the stripes were related to relative sparing of myelin in the perivenular regions in GM1 and MLD, but lipid-containing glial cells were also present in these areas in MLD. Perivenular clusters of globoid cells containing lipid material in absence of any myelin corresponded to the stripes in GLD.**

CONCLUSION: **Results of our postmortem study showed that radial stripes of white matter on MR images represented relative myelin sparing in some lysosomal storage disorders, but they may also represent lipid storage.**

MR imaging is highly sensitive in the detection of white matter lesions. On the basis of the distinct pattern of distribution of these lesions, it is possible to discriminate between a large number of different white matter disorders (1). Unfortunately, MR imaging has a limited specificity with regard to the underlying pathology of white matter abnormalities (2).

Previous reports of MR imaging studies in patients with metachromatic leukodystrophy (MLD) and globoid cell leukodystrophy (GLD) have described symmetric diffuse high signal intensity on T2-weighted images throughout the cerebral white matter with radially oriented stripes of low signal intensity (3–6). This same characteristic MR imaging pattern can also be seen in patients with infantile GM1 gangliosidosis (GM1) (personal observations, [J.P.v.d.V., M.S.v.d.K.]). The pattern in these lysosomal storage disorders is thought to represent a lack of myelin with perivenular sparing of myelin (3–6). However, this hypothesis does not find support in published case reports on the histopathologic results of the respective disorders (7–9).

To understand the observed MR imaging findings in the three lysosomal storage disorders we conducted postmortem MR imaging and histopathologic correlative studies of brains from patients with MLD, GLD and infantile GM1, and had *in vivo* MR imaging before death.

Methods

Three patients with the three different lysosomal storage disorders—infantile GM1, MLD and GLD—were included in

Received January 19, 2004; accepted after revision June 14.

From the Departments of Child Neurology (J.P.v.d.V., M.S.v.d.K.), Pathology (J.P.v.d.V., W.K.), Physics and Medical Technology (P.J.W.P.), and Radiology (F.B.), VU University Medical Center, Amsterdam, and the Departments of Pathology and Neurology (M.L.), University Medical Center Nijmegen, the Netherlands, and the Departments of Pathology and Neurology (J.M.P.), University of Rochester School of Medicine and Dentistry, NY.

Supported by the Dutch Organization of Scientific Research (NWO, grant 903-42-097) and the Optimix Foundation for Scientific Research, the Netherlands.

Address reprint request to J. P. van der Voorn, MD, Departments of Child Neurology and Pathology, VU University Medical Center, De Boelelaan 1117, 1007 MB Amsterdam, the Netherlands.

Summary of clinical characteristics of patients

Patient/Sex	Disorder	Age at MR Imaging	Neurologic details
1/M	Infantile GM1	0 y 7 mo	Presented at age 5 mo with a failure to thrive; progressively deteriorated, with hypotonia, poor head control and poor visual contact, and died at age 13 mo
2/F	MLD	17 y 0 mo	Symptoms started at age 16 y, with walking and learning problems; died 1 mo after bone marrow transplantation at age 18 y 3 mo
3/F	GLD	0 y 6 mo, 0 y 11 mo	Feeding difficulties and poor visual response at age 3 mo; developed hypertonia, increased irritability and epilepsy; condition deteriorated rapidly and died at 1 y of age

our study (Table). All examinations were performed using a 1.5T MR unit (Vision; Siemens Erlangen, Germany). In all patients, the standard *in vivo* imaging protocol for the brain included sagittal and transverse T1-weighted (TR/TE/NEX, 570/14/2) and T2-weighted (TR/TE/NEX, 3000/22, 60, and 120/1) spin-echo images and coronal or transverse fluid-attenuated inversion recovery (FLAIR) images (TR/TE/TI/NEX, 9000/105/2200/1).

The parents signed informed consent for both postmortem MR imaging and brain autopsy. Patients were examined at autopsy within 6 hours after their death to limit the effect of autolysis. Postmortem imaging of the brain was performed after at least 5 weeks of formalin fixation. The brains were cut into 1-cm-thick coronal sections and for each patient, and four or five sections that were subjected to MR imaging were selected. The fixed, 1-cm-thick brain sections were put on plastic layers, 2 cm apart, into the brain section holder, a specially fabricated device for simultaneous MR imaging of up to seven brain sections in one session. This device fit in the MR head coil (10).

The standard postmortem imaging protocol for the fixed brain sections included T2-weighted spin-echo images, and multislab 3D FLAIR images. Imaging parameters of the postmortem T2-weighted spin-echo sequence were as follows: TR/TE/NEX, 2000/20 and 45/1; matrix, 160 × 256; field of view, 125 × 200 mm; and total acquisition time, 5 minutes. The section thickness was 5 mm, and the in-plane resolution was 1 mm^2. The imaging sections were located at the center of the brain sections. In addition, a multislab 3D FLAIR sequence was used with high spatial resolution and included six 1-cm-thick slabs with eight partitions each, resulting in a section thickness of 1.25 mm with the following parameters: TR/TE/TI, 6500/120/2200; matrix, 162 × 256; field of view, 127 × 200 mm; in-plane resolution, 0.78 × 0.78 mm; and total acquisition time, 8 minutes. It was based on a turbo spin-echo imaging sequence with a turbo factor of 27 (11, 12). The multislab nature of this sequence was used to fit the design of the box; we selected 1 cm for both the slab thickness and the gap between the slabs.

After imaging, the coronal brain-sections were cut in half by using a 5-mm deep cutting device; we ensured that the cut surface of the halved section corresponded with the imaging plane of the T2-sequence (10). Subsequently, the sections were embedded in paraffin, and whole-mount 7-μm-thick sections were made. Routine neuropathologic staining techniques were applied to these paraffin sections, including hematoxylin and eosin staining and Luxol fast blue staining to delineate areas of myelin breakdown and Bodian silver impregnations to determine axonal attenuation. Immunohistochemical staining was performed on selected 5-μm-thick paraffin-embedded sections by using the streptavidin-biotin complex procedure. The following primary antibodies were used: macrophage-specific marker KP1 (CD68) and leukocyte common antigen (CD45) to detect inflammatory cells and glial fibrillary acidic protein (GFAP) to evaluate the intensity of astrogliosis. The sections stained with hematoxylin and eosin were used to verify whether the histologic sections matched the contours of the corresponding MR images. The areas corresponding to hypointense stripes on the 3D FLAIR post mortem MR images were specifically compared with the matched areas on the histologic sections.

Results

Figures 1, 2, and 3 show *in vivo,* postmortem, and histopathologic images of the patients with GM1, MLD, and GLD patients, respectively.

In vivo T2-weighted images demonstrated a diffuse and symmetrical increase in signal intensity throughout the cerebral white matter in all three patients. In the affected white matter dots and stripes with low signal intensity were seen (comparable to findings in myelinated white matter), with a punctate pattern on the superior and a radial pattern on the inferior transverse T2-weighted images. Coronal FLAIR images displayed a pattern of radial stripes of low signal intensity within the hyperintense white matter; the stripes extended from the cerebral cortex to the ventricular wall. On the T1-weighted images, the stripes had a normal high signal intensity, whereas the remainder of the cerebral white matter had an abnormally low signal intensity. The stripes were more prominent in patients with GLD and MLD than in the patient with GM1.

T2-weighted and 3D FLAIR images obtained in the formalin-fixed coronal brain sections of the three patients revealed similar MR findings: a hyperintense centrum semiovale with radially oriented stripes of relatively normal, hypointense signal intensity.

Neuropathologic evaluation of the white matter in GM1 demonstrated a diffuse paucity of myelin on LFB-stained sections and a commensurate loss of oligodendrocytes with relative sparing of axons on Bodian silver impregnations. Mild astrogliosis was observed in the white matter, with a few CD68-positive macrophages. Microscopic study of the matched LFB-stained sections showed that the hypointense stripes on MR imaging represented perivenular areas of relatively increased myelin within the otherwise

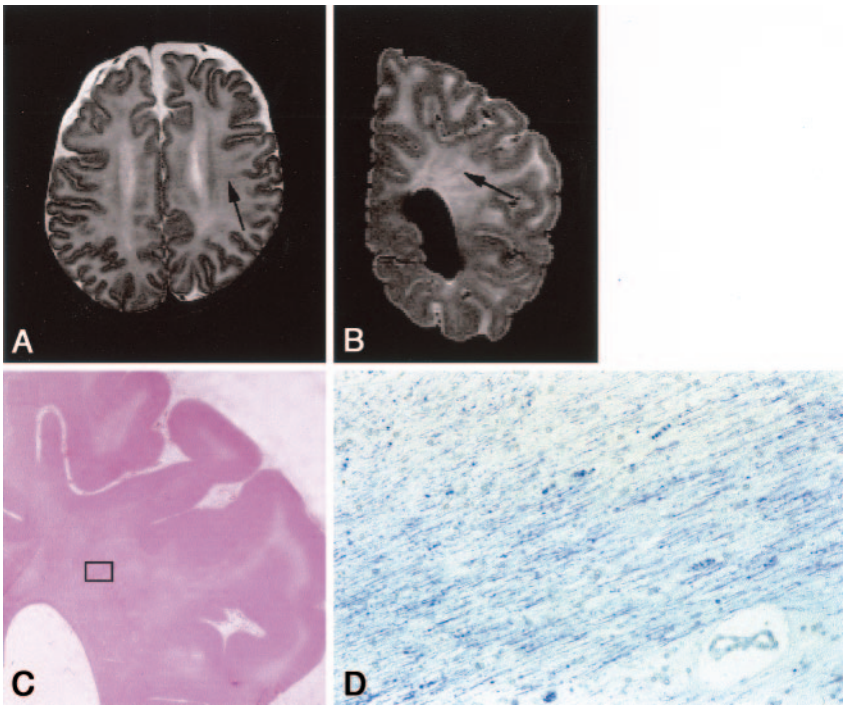

FIG 1. Patient 1, who had GM1.

A and *B*, *In vivo* transverse T2-weighted image (*A*) and postmortem coronal 3D FLAIR image (*B*) show a diffuse and symmetric increase in signal intensity in the cerebral white matter, with radial stripes of low signal intensity (*arrows*).

C and *D*, Photomicrograph (hematoxylin and eosin, original magnification ×1.5) of a matched histopathologic section (*C*) and magnified view (Luxol fast blue, original magnification ×75) of the small box in *C* (*D*) reveal perivenular areas of relatively normal density of myelin sheaths (*blue* in *D*) in the hypomyelinated central white matter (*top left* and *bottom right* in *D*); these areas corresponding to the hypointense stripes on MR imaging.

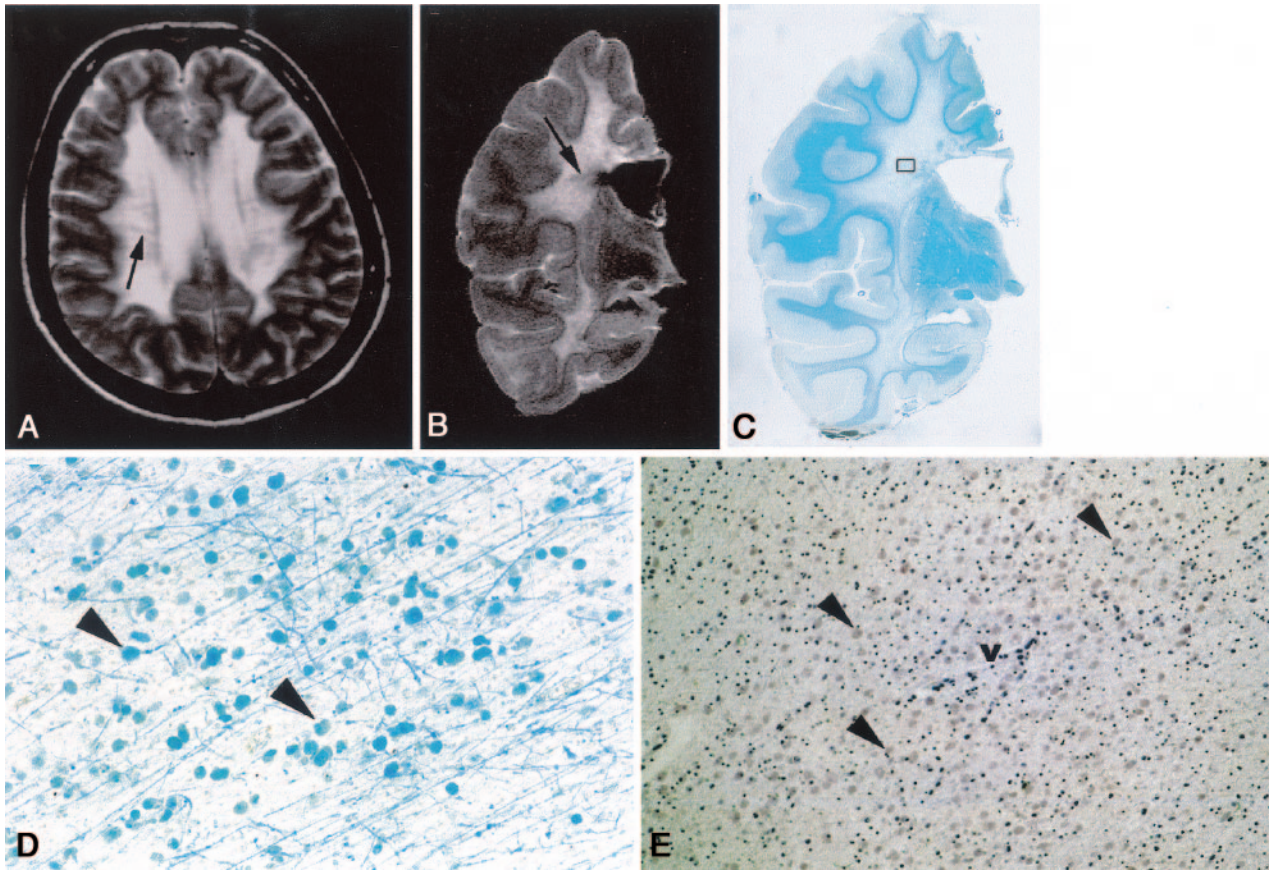

FIG 2. Patient 2, who had MLD.

A and *B*, *In vivo* transverse T2-weighted image (*A*) and postmortem coronal 3D FLAIR image (*B*) show a hyperintense centrum semiovale with radially oriented stripes of hypointense signal intensity (*arrows*).

C, Photomicrograph (Luxol fast blue, original magnification ×1) demonstrates a profound absence of myelin throughout the centrum semiovale with some sparing of the areas of subcortical U fibers.

D and *E*, Magnified views of hematoxylin and eosin (*D*, original magnification ×37.5) and Luxol fast blue (*E*, original magnification ×75) stains of the small box in *C* show that the hypointense linear bands correspond with numerous eosinophilic granule containing glial cells and macrophages (*arrowheads*) around venules (*v*) and myelin (*blue stripes* in *E*).

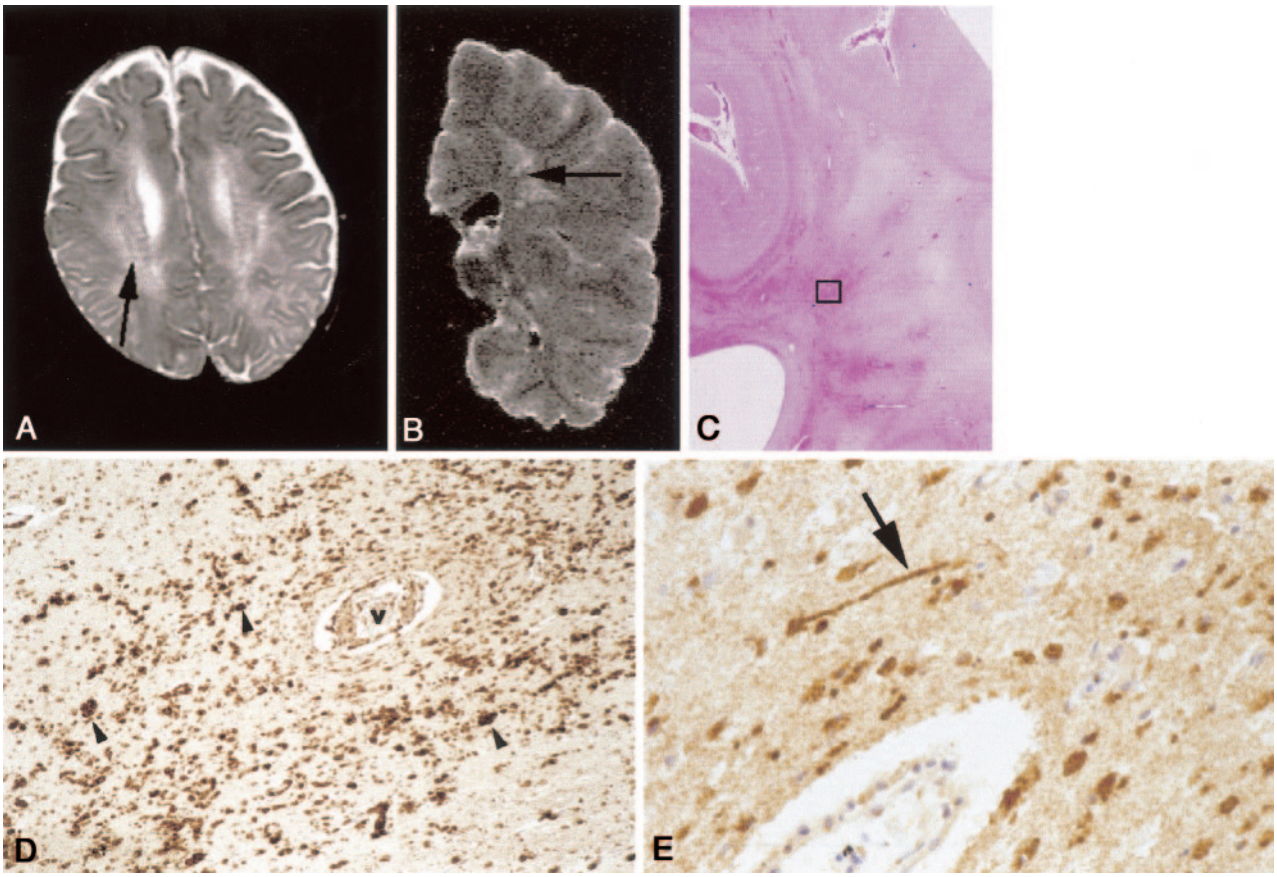

FIG 3. Patient 3, who had GLD.

A and *B*, *In vivo* transverse T2-weighted image (*A*) and postmortem coronal 3D FLAIR image (*B*) show an atrophic brain with hyperintense white matter and linear areas of hypointense signal intensity, extending from the cerebral cortex to the ventricular wall (*arrow*).

C and *D*, Photomicrograph of hematoxylin and eosin stain (*C*, original magnification, ×1.5) and magnified view of CD68 stain (*D*, original magnification ×37.5) of the small box in *C* show perivascular clustering of multinucleated globoid cells (*arrowheads*, *v* = venule).

E, MBP stain (original magnification ×75) shows almost complete absence of myelin sheaths (*arrow*).

hypomyelinated central white matter. In these areas, oligodendrocytes were better preserved (Fig 1).

The major neuropathologic changes in the MLD brain consisted of extensive demyelination throughout the white matter with some sparing of the subcortical U fibers and with numerous reactive astrocytes and macrophages with eosinophilic granules. Exact correlation of the 3D FLAIR images with LFB-stained sections showed that the hypointense bands corresponded with perivenular areas of myelin. Lipid containing glial cells and macrophages were also clustered in these areas of myelin (Fig 2).

Neuropathologic examination of the atrophic GLD brain was characterized by diffuse-to-nearly complete loss of myelin and dense astrogliosis. In these areas, marked axonal loss was seen and oligodendrocytes were diminished. Multinucleated globoid cells (cells of phagocytic lineage containing large amounts of lipids) were clustered around blood vessels. The areas of hyperintensity on T2-weighted MR imaging corresponded to myelin-deficient foci and the hypointense stripes corresponded to the perivascular clustering of globoid cells, and not to (relatively preserved) myelin (Fig 3).

Discussion

We describe a peculiar MR imaging appearance consisting of radially oriented stripes of apparently normal signal intensity within otherwise diffusely abnormal cerebral white matter in three patients with lysosomal diseases. These stripes are characteristic of these lysosomal storage disorders; they are not seen in other diffuse leukoencephalopathies. They differ from the radiating stripes within the abnormal white matter typically seen in vanishing white matter (13, 14), in which the cerebral white matter becomes rarefied and cystic. Within the rarefied and cystic white matter, which has a low signal intensity on proton attenuation and FLAIR images, radiating stripes of remaining tissues strands are seen, but the stripes have an abnormally high signal intensity. The stripes in vanishing white matter are not visible on T2-weighted images because both the rarefied and cystic white matter and the strands of abnormal tissues have a high signal intensity (13, 14).

The stripes in lysosomal storage disorders were thought to represent perivenular sparing of myelin (3–6), but to our knowledge, their nature has not

been investigated before. We performed postmortem MR imaging with histopathologic correlation to understand the neuropathologic basis underlying this MR imaging pattern. Similar imaging features were found in the three examined patients on *in vivo* and postmortem imaging. The MR imaging visible stripes were subtle in GM1. Histopathologic studies confirmed that the stripes were related to relative presence of myelin in this disease. The stripes visible on MR imaging were more prominent in GLD and MLD, and histopathologic studies showed that the situation was more complex in these disorders. In MLD, the perivenular regions, which corresponding to the stripes on MR imaging, myelin was relatively more prominent. However, these areas also had an accumulation of glial cells and macrophages containing lipids. In GLD, many globoid cells containing lipid material in the perivenular regions, in the absence of any myelin, corresponded to the stripes on MR imaging. The high cell density and, most of all, the high content of stored lipids in these cell, most likely contribute to shortening of both T2 and T1 values.

Postmortem MR imaging of formalin-fixed brain specimens can be easily performed on a standard MR imaging machine. The multislab 3D FLAIR sequence, which has been used to detect lesions in patients with multiple sclerosis (11, 12), provides thin sections with a high signal-to-noise ratio and allows direct histopathologic correlation with signal intensity abnormalities on MR imaging.

The findings at postmortem MR imaging, performed after formalin fixation, were qualitatively well correlated with the *in vivo* imaging findings. Formalin interposes itself between side groups of certain amino acids, causing cross-linking and restricting mobility of molecules in the tissue after fixation. After tissue fixation in formalin, T1 and T2 relaxation times are reduced with the most rapid changes during the first 1–2 weeks, reaching a plateau by the 5th week (15–18). For this reason, we used slightly adapted TEs (shorter relative to *in vivo* studies) during T2-weighted imaging for the study of formalin-fixed tissue. Despite the shortening of T1 and T2 relaxation times secondary to formalin fixation, the gray matter–white matter differentiation and heterogeneity of signal intensity in the white matter remained evident on postmortem T2-weighted imaging.

The multislab 3D FLAIR sequence was used in the postmortem MR imaging protocol to obtain thin sections, which allowed good matching with the whole-mount histopathologic sections. However, 3D FLAIR imaging is not essential to demonstrate the stripes *in vivo* in patients with these lysosomal white matter disorders. Conventional T2-weighted imaging on a standard scanner also reveals the stripes in the diffusely affected white matter, which may be helpful in distinguishing these disorders from other leukoencephalopathies.

Conclusion

Our results show that different histopathologic correlates are responsible for a similar characteristic MR imaging pattern in three lysosomal storage disorders. Postmortem imaging followed by correlative histopathologic tests can help to elucidate the histopathologic basis of imaging features in white matter disorders.

Acknowledgments

We thank Hugo Vrenken for his assistance in the postmortem MR imaging measurements. We are also grateful to Jaap van Veldhuisen and Ron Otsen for their artistic graphic support.

References

1. Van der Knaap MS, Breiter SN, Naidu S, et al. **Defining and categorizing leukoencephalopathies of unknown origin: MR imaging approach.** *Radiology* 1999;213:121–133
2. Van der Knaap MS. **Magnetic resonance in childhood white-matter disorders.** *Dev Med Child Neurol* 2001;43:705–712
3. Faerber EN, Melvin JJ, Smergel EM. **MRI appearances of metachromatic leukodystrophy.** *Pediatr Radiol* 1999;29:669–672
4. Kim IO, Kim WS. **MR of childhood metachromatic leukodystrophy.** *AJNR Am J Neuroradiol* 1997;18:733–738
5. Sasaki M, Sakuragawa N, Takashima S, Hanaoka S. **MRI and CT findings in Krabbe disease.** *Pediatr Neurol* 1991;7:283–288
6. Barkovich AJ. **Concepts of myelin and myelination in neuroradiology.** *AJNR Am J Neuroradiol* 2000;21:1099–1109
7. Folkerth RD, Alroy J, Bhan I, Kaye EM. **Infantile GM1 gangliosidosis: complete morphology and histochemistry of two autopsy cases with particular reference to delayed central nervous system myelination.** *Pediatr Dev Pathol* 2000;3:73–86
8. Haberland C, Brunngraber E, Witting L, Daniels A. **Juvenile metachromatic leukodystrophy: case report with clinical, histopathological, ultrastructural and biochemical observations.** *Acta Neuropathol* 1973;26:93–106
9. Percy AK, Odrezin GT, Knowles PD, Rouah E, Armstrong DD. **Globoid cell leukodystrophy: comparison of neuropathology with magnetic resonance imaging.** *Acta Neuropathol* 1994;88:26–32
10. Bö L. Geurts JJG, Ravid R, Barkhof F. **Magnetic resonance imaging as a tool to examine the neuropathology of multiple sclerosis.** *Neuropathol Appl Neurobiol* 2004;2:106–17
11. Tan IL, Pouwels PJ, van Schijndel RA, Ader HJ, Manoliu RA, Barkhof F. **Isotropic 3D fast FLAIR imaging of the brain in multiple sclerosis patients: initial experience.** *Eur Radiol* 2002;12:559–567
12. Tan IL, van Schijndel RA, Pouwels PJ, Ader HJ, Barkhof F. **Serial isotropic three-dimensional fast FLAIR imaging: using image registration and subtraction to reveal active multiple sclerosis lesions.** *AJR Am J Roentgenol* 2002;179:777–782
13. Van der Knaap MS, Barth PG, Gabreëls FJM, et al. **A new leukoencephalopathy with vanishing white matter.** *Neurology* 1997;48:845–855
14. Van der Knaap MS, Kamphorst W, Barth PG, Kraaijeveld CL, Gut E, Valk J. **Phenotypic variation in leukoencephalopathy with vanishing white matter.** *Neurology* 1998;51:540–547
15. Tovi M, and Ericsson A. **Measurements of T1 and T2 over time in formalin-fixed human whole-brain specimens.** *Acta Radiol* 1992;33:400–404
16. Blamire AM, Rowe JG, Styles P, McDonald B. **Optimising imaging parameters for post mortem MR imaging of the human brain.** *Acta Radiol* 1999;40:593–597
17. Thickman DI, Kundel HL, Wolf G. **Nuclear magnetic resonance characteristics of fresh and fixed tissue: the effect of elapsed time.** *Radiology* 1983;148:183–185
18. Van den Hauwe L, Parizel PM, Martin JJ, Cras P, De Deyn P, De Schepper AMA. **Postmortem MRI of the brain with neuropathological correlation.** *Neuroradiology* 1995;37:343–349.